Verification of the improved chemistry solver

This material provides comparisons between standard solvers and improved solvers to verify the numerical consistency of the improved solvers with OpenFOAM-10. The comparisons include zero-dimensional constant pressure auto ignition and two-dimensional counter flow flame.

1. Zero-dimensional constant pressure auto ignition

Three ODE solvers, including Rodas34 algorithm, Rosenbrock34 algorithm and Seulex algorithm are selected for numerical verification. The ignition is solved using appilication chemFoam in foundation version OpenFOAM-10. The absolute tolerance and relative tolerance are 10^{-12} and 10^{-6}, respectively. The result using OpenFOAM standard chemistry solver and the improved chemistry solver is compared.

1.1 Hydrogen

Table S1. Operating condition of hydrogen/air constant pressure auto ignition

Size	T_0 (K)	P_0 (Pa)	Refs
10s21r	1200	101325	[1]
15s75r	1200	101325	[2]

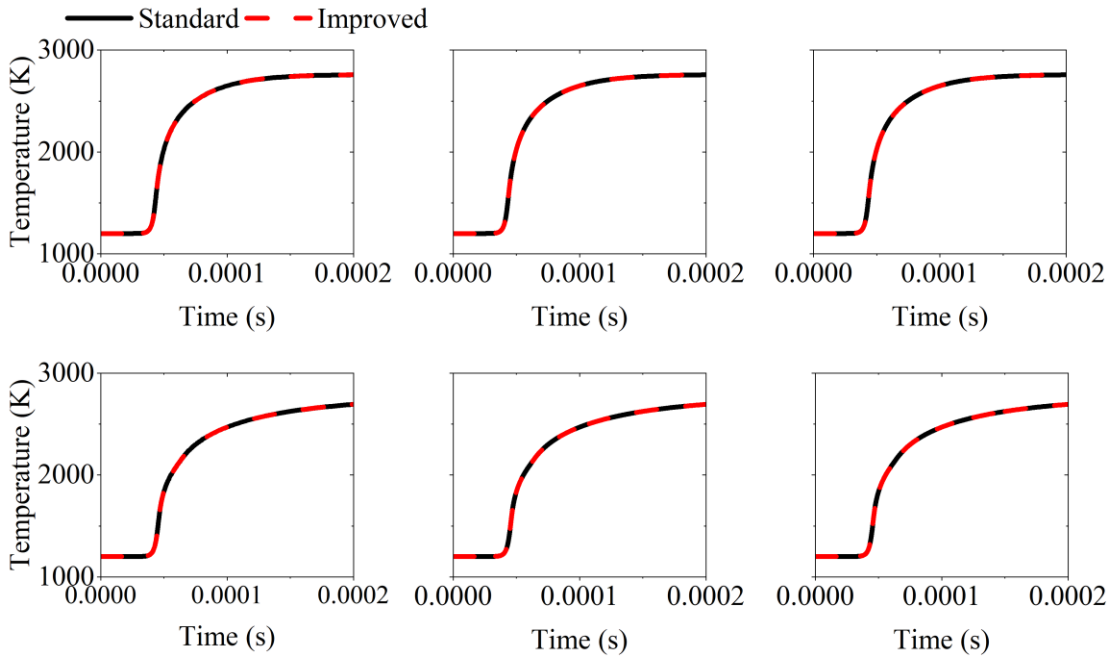

Fig. S1. Temperature profiles for hydrogen/air under constant-pressure autoignition conditions. The first row: 10s21r, the second row: 15s75r. Left: Rodas34 algorithm, middle: Rosenbrock34 algorithm, right: Seulex algorithm.

1.2 Methane

Table S2. Operating condition of methane/air constant pressure auto ignition

Size	T_0 (K)	P_0 (Pa)	Refs
22s104r	1000	136789	[3]
53s325r	1000	136789	[4]

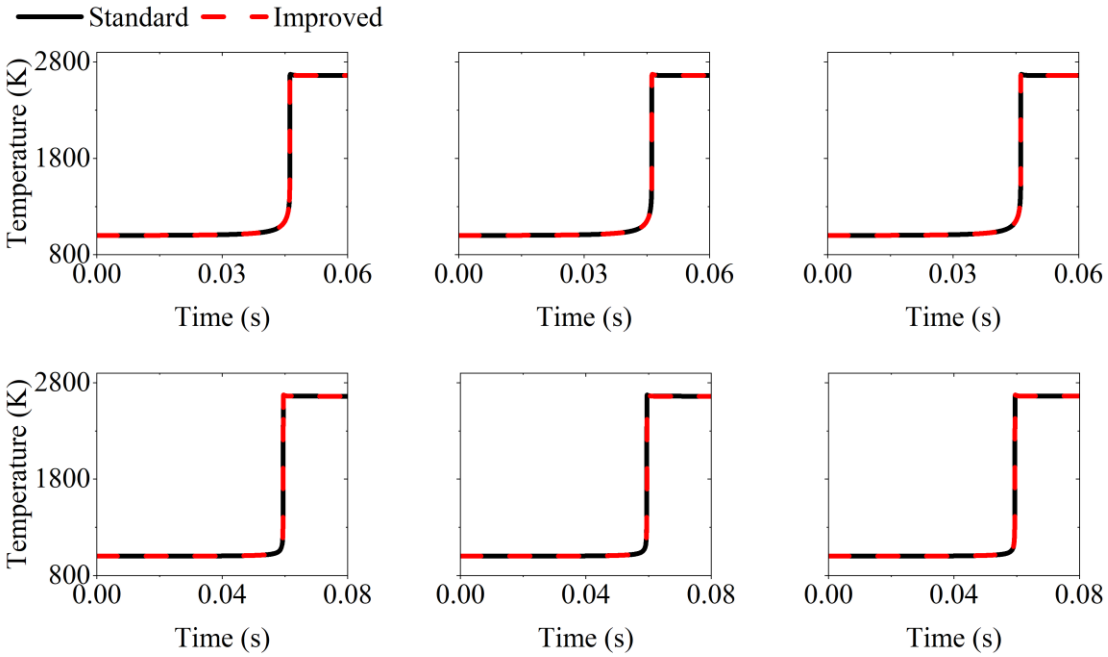

Fig. S2. Temperature profiles for methane/air under constant-pressure autoignition conditions. The first row: 10s21r, the second row: 15s75r. Left: Rodas34 algorithm, Middle: Rosenbrock34 algorithm, right: Seulex algorithm.

1.3 Ethylene

Table S3. Operating condition of ethylene /air constant pressure auto ignition

Size	T_0 (K)	P_0 (Pa)	Refs
24s70r	1000	202650	[5]
59s268r	1000	202650	[6]

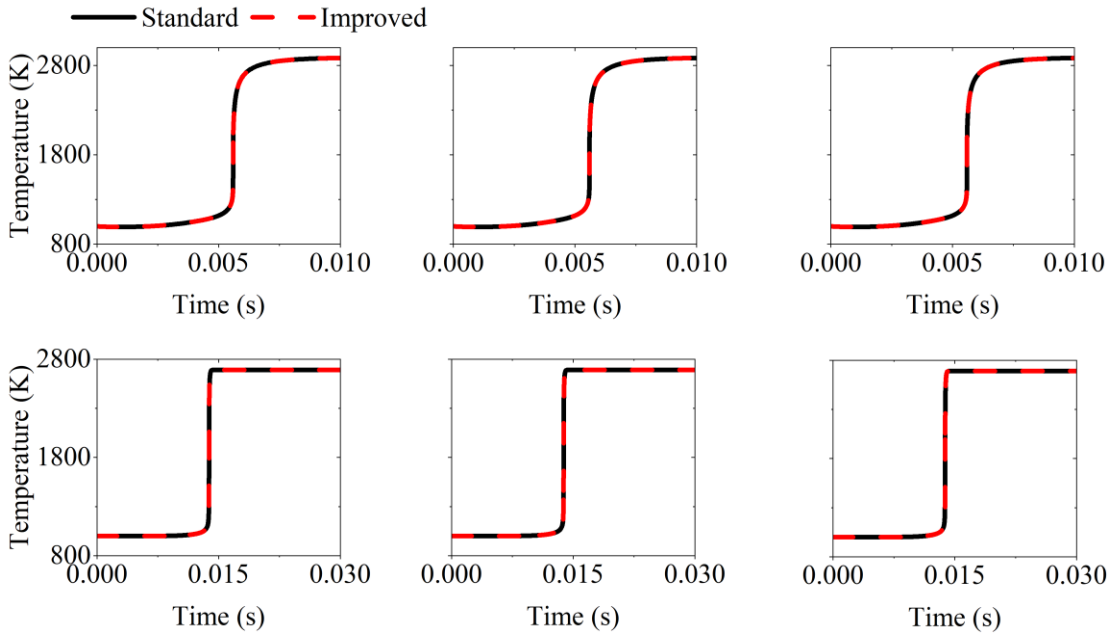

Fig. S3. Temperature profiles for ethylene/air under constant-pressure autoignition conditions. The first row: 24s70r, the second row: 59s268r. Left: Rodas34 algorithm, Middle: Rosenbrock34 algorithm, right: Seulex algorithm.

1.4 Ethanol

Table S4. Operating condition of ethanol/air constant pressure auto ignition

Size	T_0 (K)	P_0 (Pa)	Refs
39s379r	1000	202650	[7]
57s383r	1000	202650	[8]

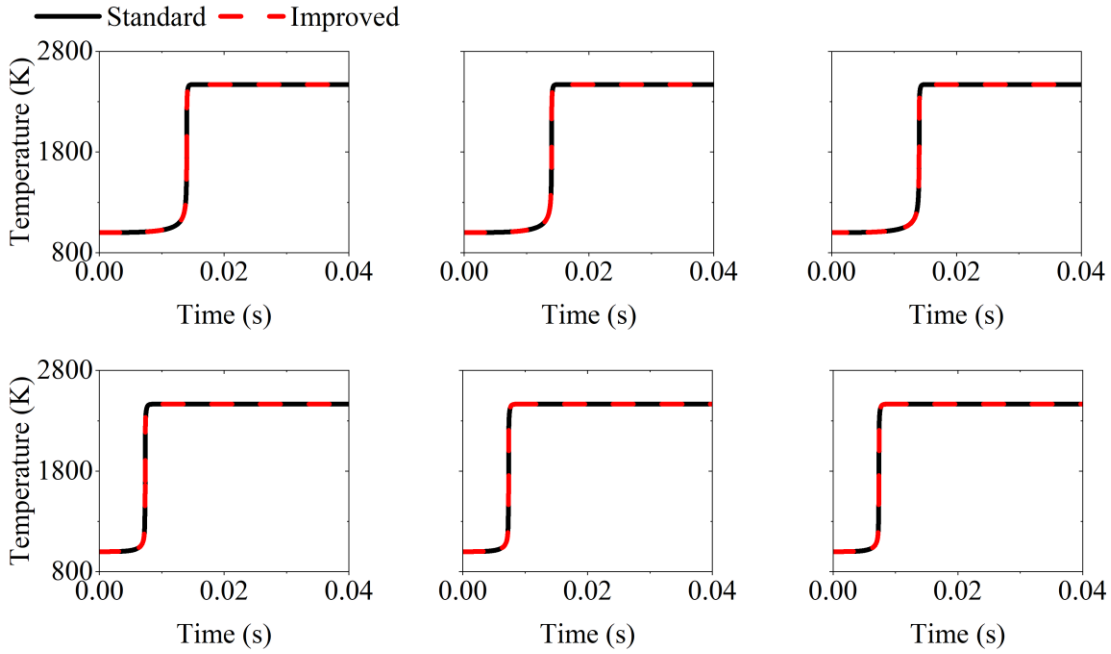

Fig. S4. Temperature profiles for ethanol/air under constant-pressure autoignition conditions. The

first row: 39s379r, the second row: 57s383r. Left: Rodas34 algorithm, Middle: Rosenbrock34 algorithm, right: Seulex algorithm.

1.5 N-heptane

Table S5. Operating condition of n-heptane/air constant pressure auto ignition

Size	T_0 (K)	P_0 (Pa)	Refs
46s115r	700	2000000	[9]
68s283r	700	2000000	[10]
188s939r	700	2000000	[11]

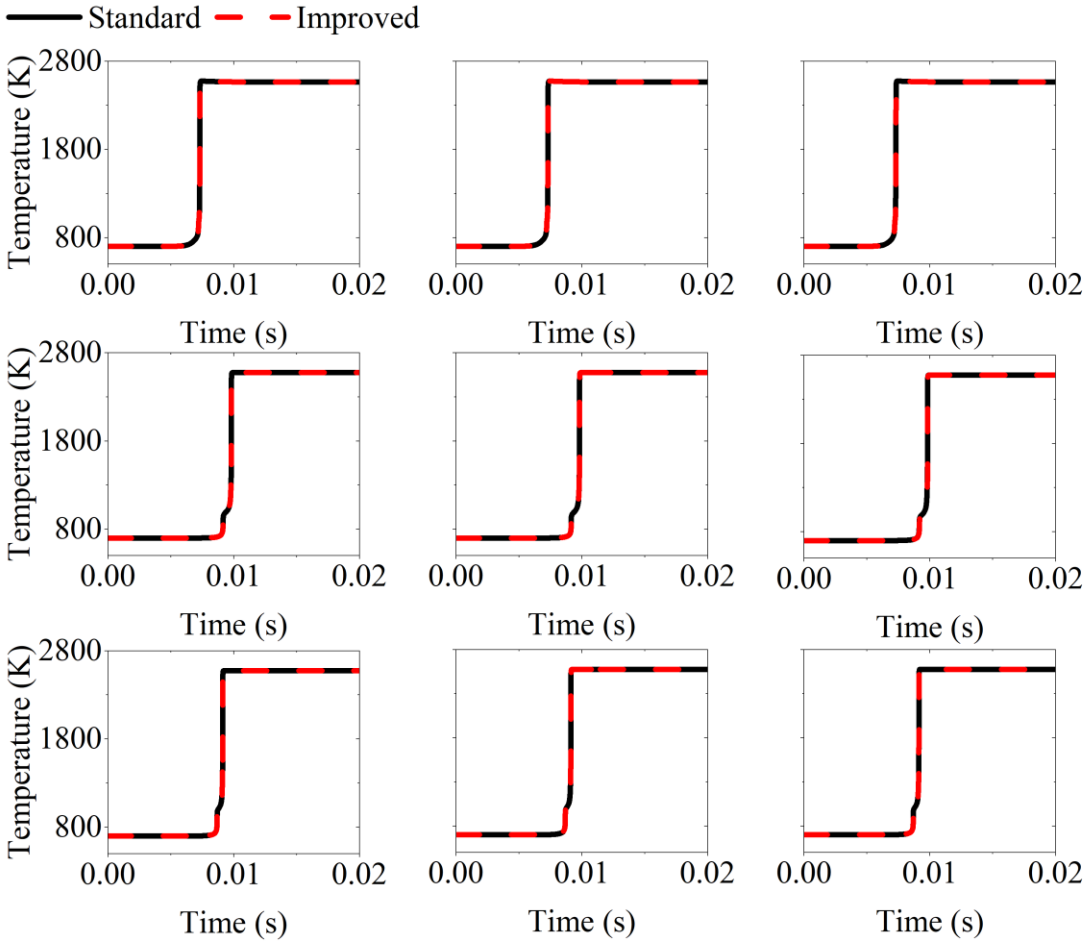

Fig. S5. Temperature profiles for n-heptane/air under constant-pressure autoignition conditions. The first row: 46s115r, the second row: 68s283r, the third row: 188s939r. Left: Rodas34 algorithm, middle: Rosenbrock34 algorithm, right: Seulex algorithm.

1.6 N-dodecane

Table S6. Operating condition of n-dodecane/air constant pressure auto ignition

Size	T_0 (K)	P_0 (Pa)	Refs
31s193r	1000	2000000	[12]
54s268r	1000	2000000	[13]

255s1509r	1000	2000000	[14]

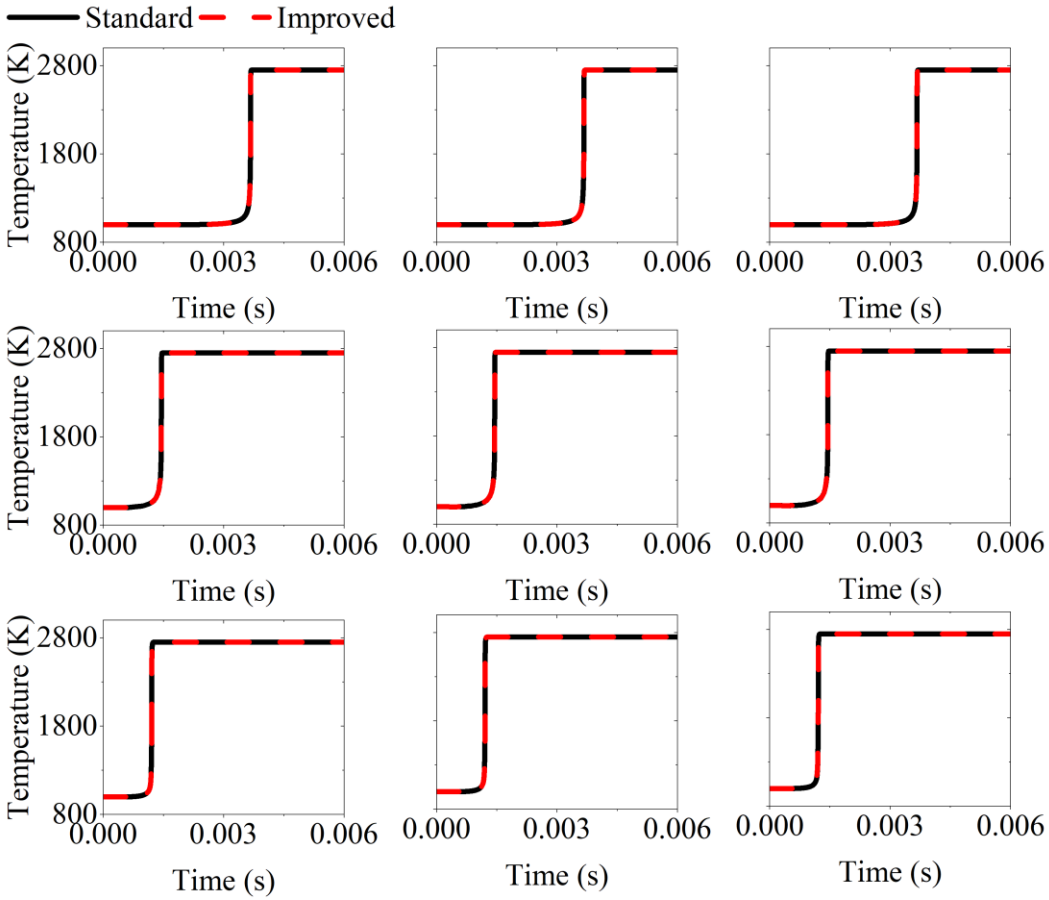

Fig. S6. Temperature profiles for n-heptane/air under constant-pressure autoignition conditions. The first row: 31s193r, the second row: 54s268r, the third row: 255s1509r. Left: Rodas34 algorithm, middle: Rosenbrock34 algorithm, right: Seulex algorithm.

1.7 Iso-octane

Table S7. Operating condition of iso-octane/air constant pressure auto ignition

Size	T_0 (K)	P_0 (Pa)	Refs
140s643r	700	2000000	[15]
874s3796r	700	2000000	[16]

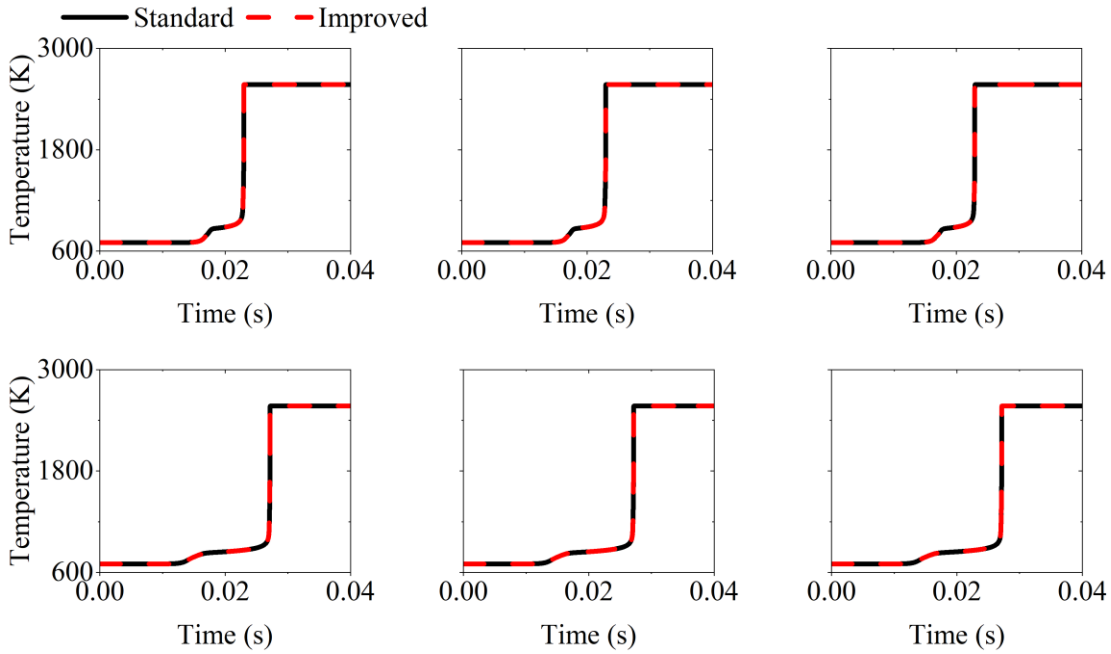

Fig. S7. Temperature profiles for iso-octane/air under constant-pressure autoignition conditions. The first row: 140s643r, the second row: 874s3796r. Left: Rodas34 algorithm, middle: Rosenbrock34 algorithm, right: Seulex algorithm.

1.8 Kerosene

Table S8. Operating condition of kerosene/air constant pressure auto ignition

Size	T_0 (K)	P_0 (Pa)	Refs
30s77r	800	2000000	[17]
28s92r	1100	2000000	[18]

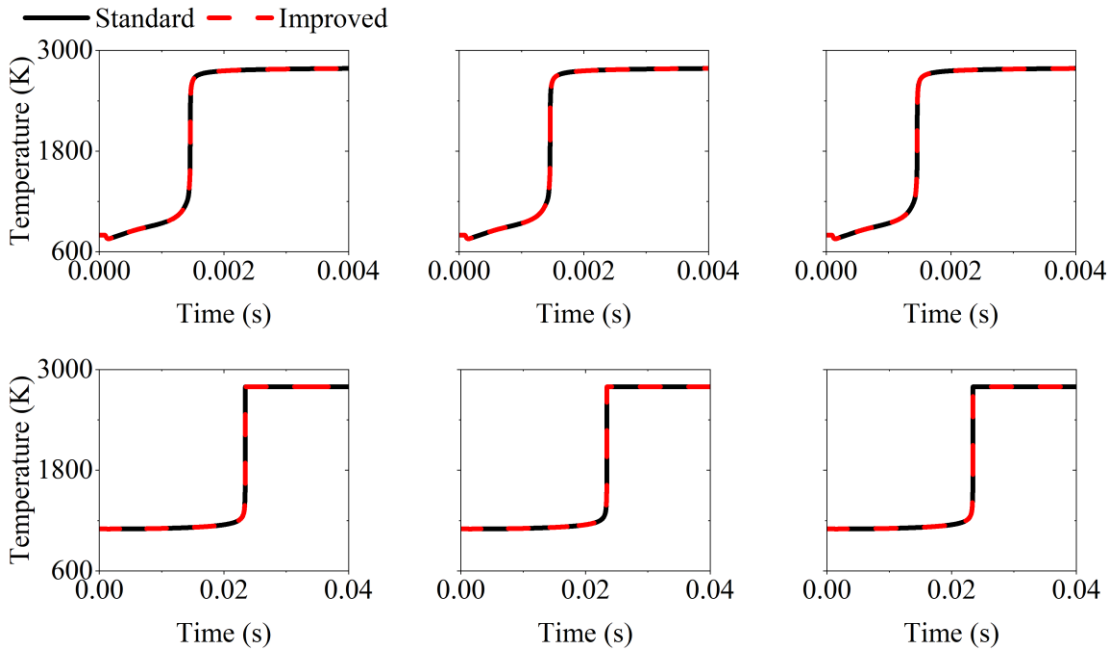

Fig. S8. Temperature profiles for kerosene/air under constant-pressure autoignition conditions. The first row: 30s77r, the second row: 28s92r. Left: Rodas34 algorithm, middle: Rosenbrock34 algorithm, right: Seulex algorithm.

1.9 Dimethyl Ether

Table S9. Operating condition of dimethyl ether/air constant pressure auto ignition

Size	T_0 (K)	P_0 (Pa)	Refs
26s71r	700	2000000	[19]
39s175r	700	2000000	[20]
79s351r	700	2000000	[21]

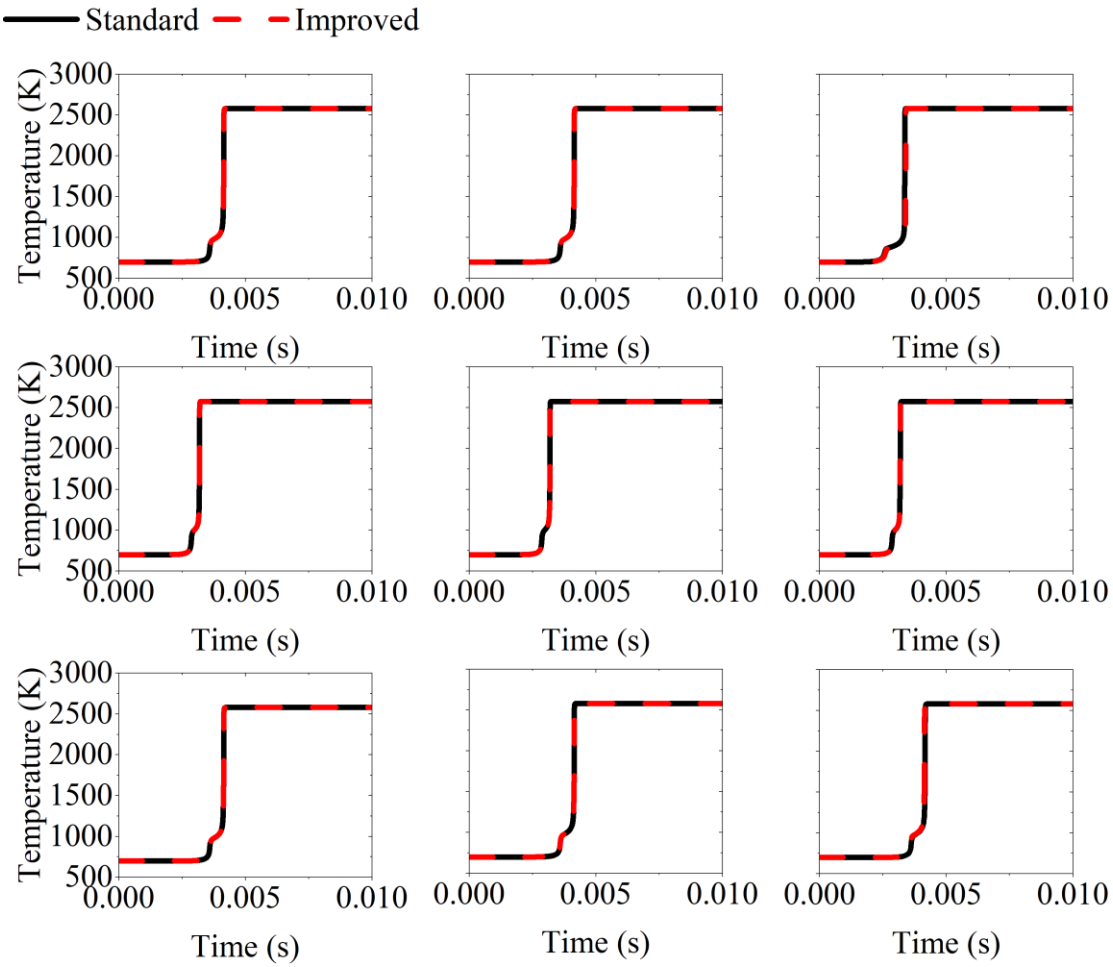

Fig. S9. Temperature profiles for dimethyl ether/air under constant-pressure autoignition conditions. The first row: 26s71r, the second row: 39s175r, the third row: 79s351r. Left: Rodas34 algorithm, middle: Rosenbrock34 algorithm, right: Seulex algorithm.

1.10 Ammonia

Table S10. Operating condition of ammonia/air constant pressure auto ignition

Size	T_0 (K)	P_0 (Pa)	Refs
59s356r	1300	100000	[22]

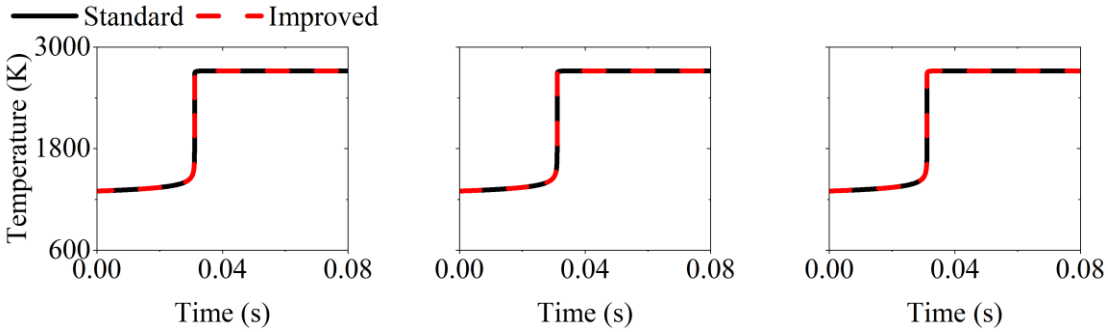

Fig. S10. Temperature profiles for ammonia/air under constant-pressure autoignition conditions. Left: Rodas34 algorithm, middle: Rosenbrock34 algorithm, right: Seulex algorithm.

2. Two-dimensional counter flow flame

Three ODE solvers, including Rodas34 algorithm, Rosenbrock34 algorithm and Seulex algorithm are selected for numerical verification. The counter flow flame is solved using appilication reactingFoam in foundation version OpenFOAM-10. The absolute tolerance and relative tolerance are 10^{-8} and 10^{-4}, respectively. The result using OpenFOAM standard chemistry solver and the improved chemistry solver is compared.

Table S11. Operating condition of methane/air counter flow flame

fuel	T_{fuel} (K)	T_{air} (K)	U_{fuel} (m/s)	U_{air} (m/s)	P_{env} (Pa)	Chemistry mechanism
methane	293	293	0.1	0.1	100000	[22]
ammonia	293	293	0.1	0.1	100000	[23]
n-dodecane	500	500	0.1	0.1	100000	[13]

2.1 Methane

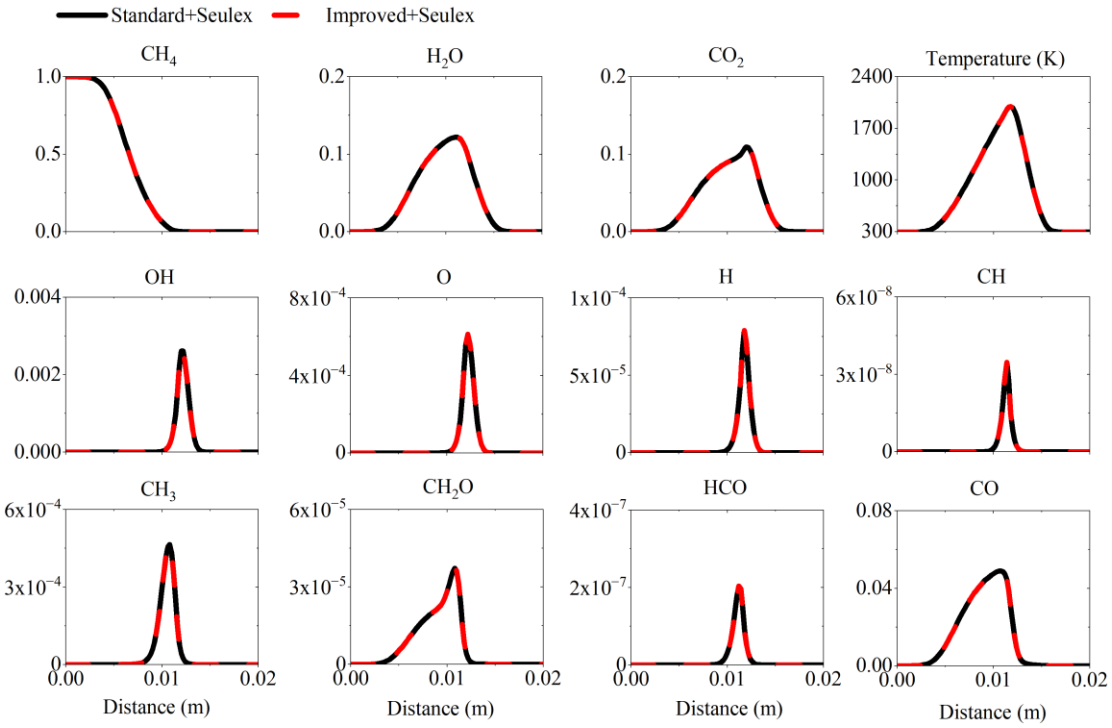

Fig. S11. Species mass fraction and temperature (K) profiles for counter flow flame of methane/air. The ODE algorithm is Seulex.

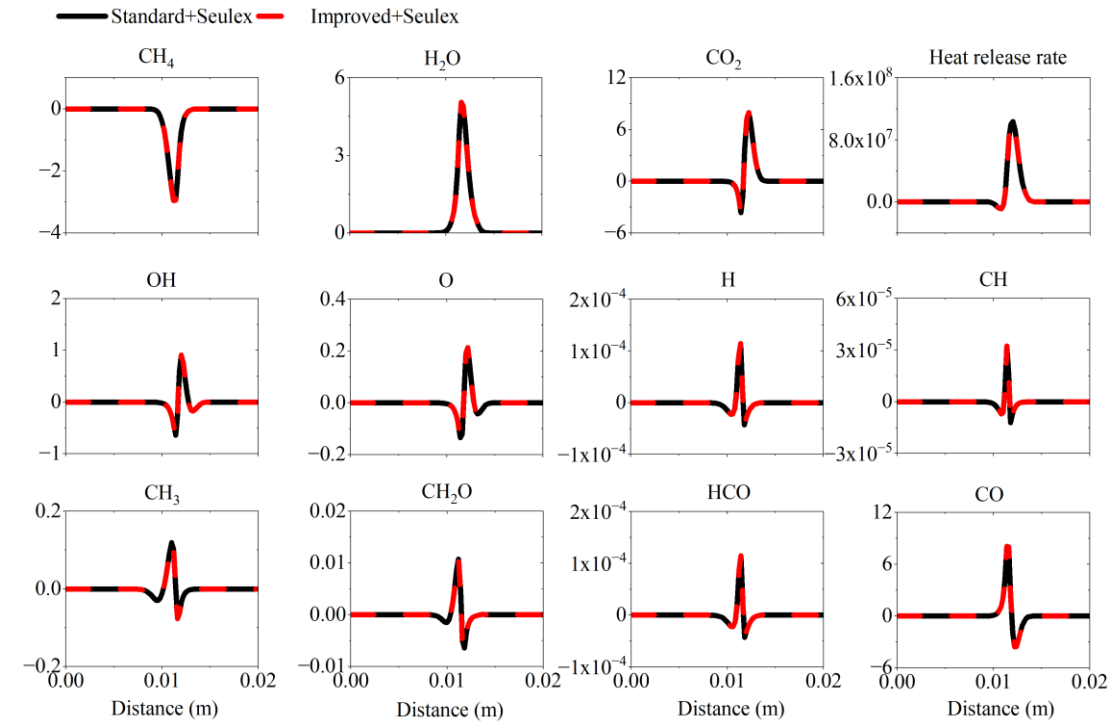

Fig. S12. Species production rate (kg/m^3/s) and heat release rate (W/m^3) profiles for counter flow flame of methane/air. The ODE algorithm is Seulex.

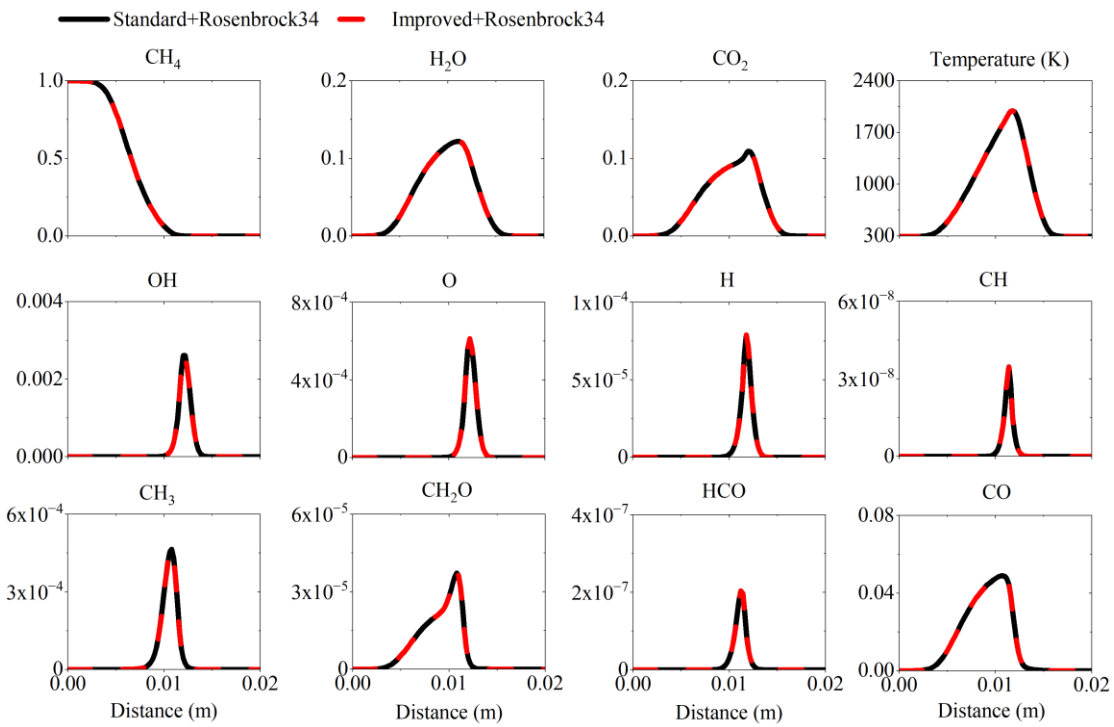

Fig. S13. Species mass fraction and temperature (K) profiles for counter flow flame of methane/air. The ODE algorithm is Rosenbrock34.

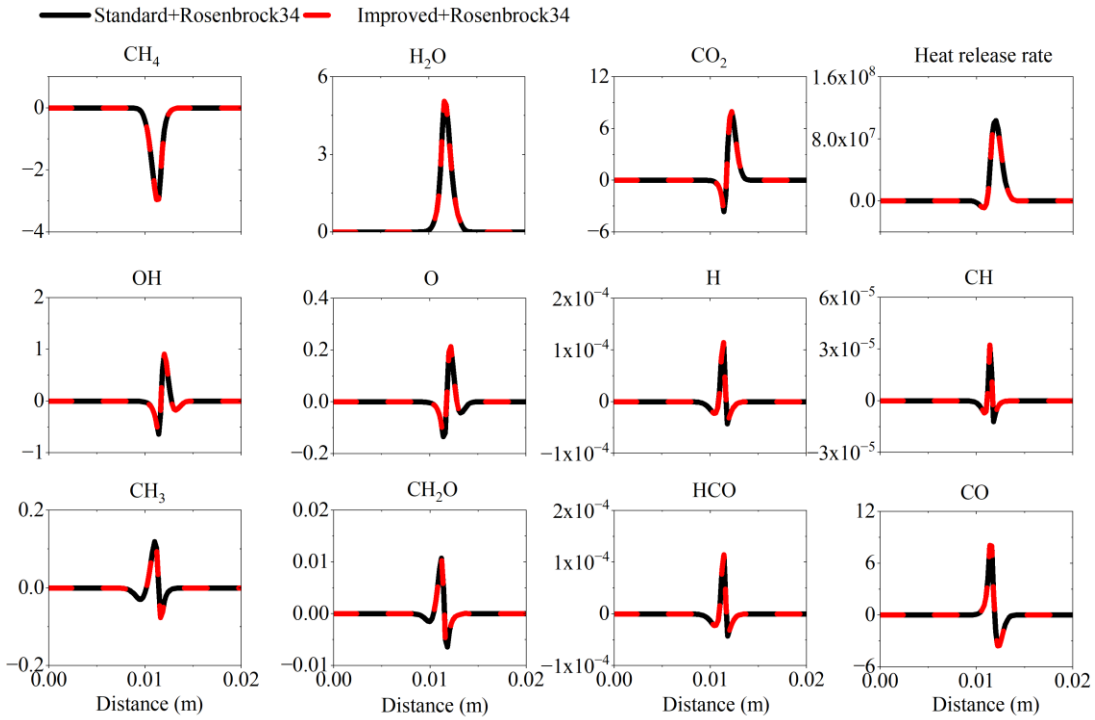

Fig. S14. Species production rate (kg/m^3/s) and heat release rate (W/m^3) profiles for counter flow flame of methane/air. The ODE algorithm is Rosenbrock34.

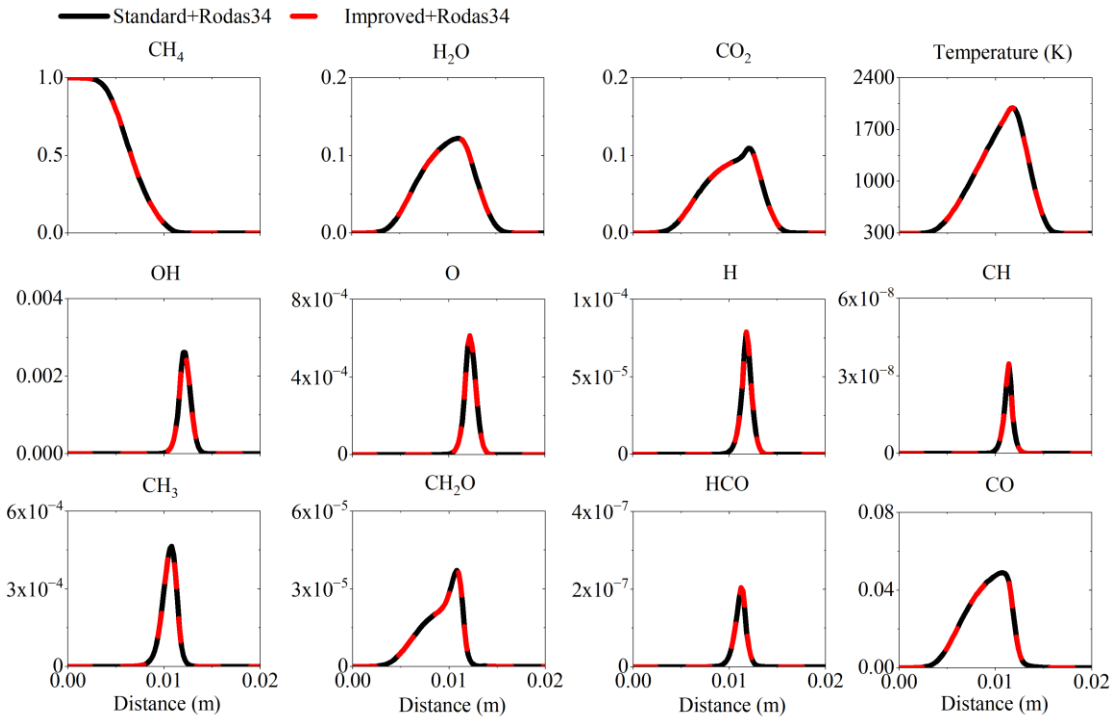

Fig. S15. Species mass fraction and temperature (K) profiles for counter flow flame of methane/air. The ODE algorithm is Rodas34.

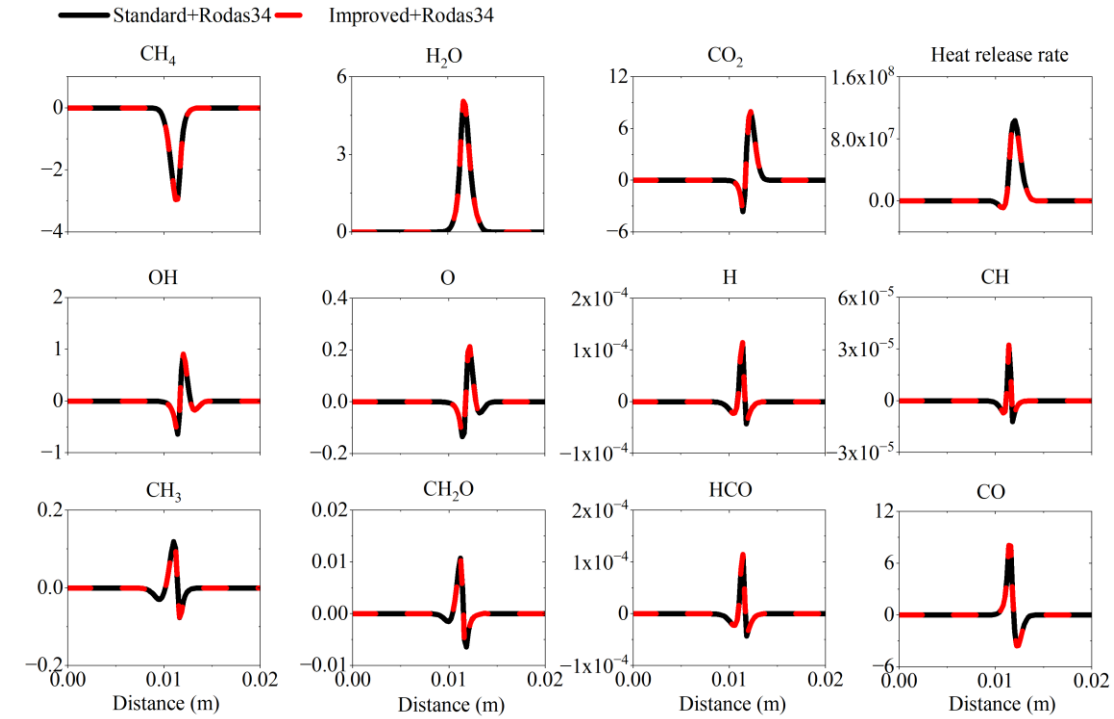

Fig. S16. Species production rate (kg/m^3/s) and heat release rate (W/m^3) profiles for counter flow flame of methane/air. The ODE algorithm is Rodas34.

2.2 Ammonia

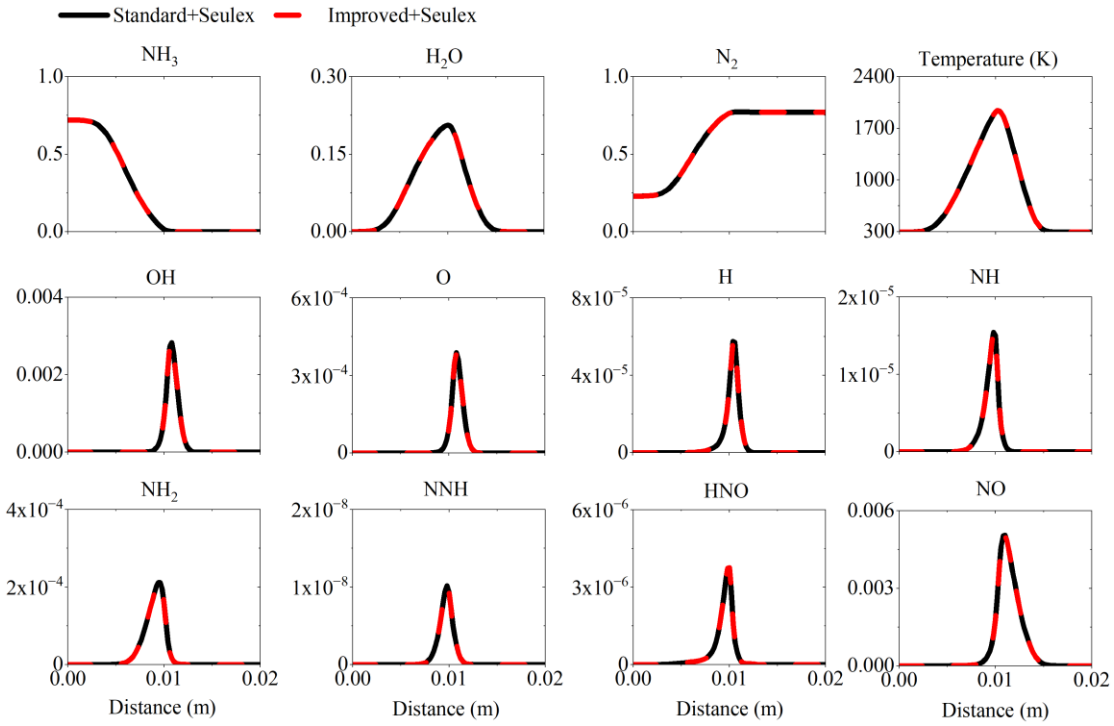

Fig. S17. Species mass fraction and temperature (K) profiles for counter flow flame of ammonia/air. The ODE algorithm is Seulex.

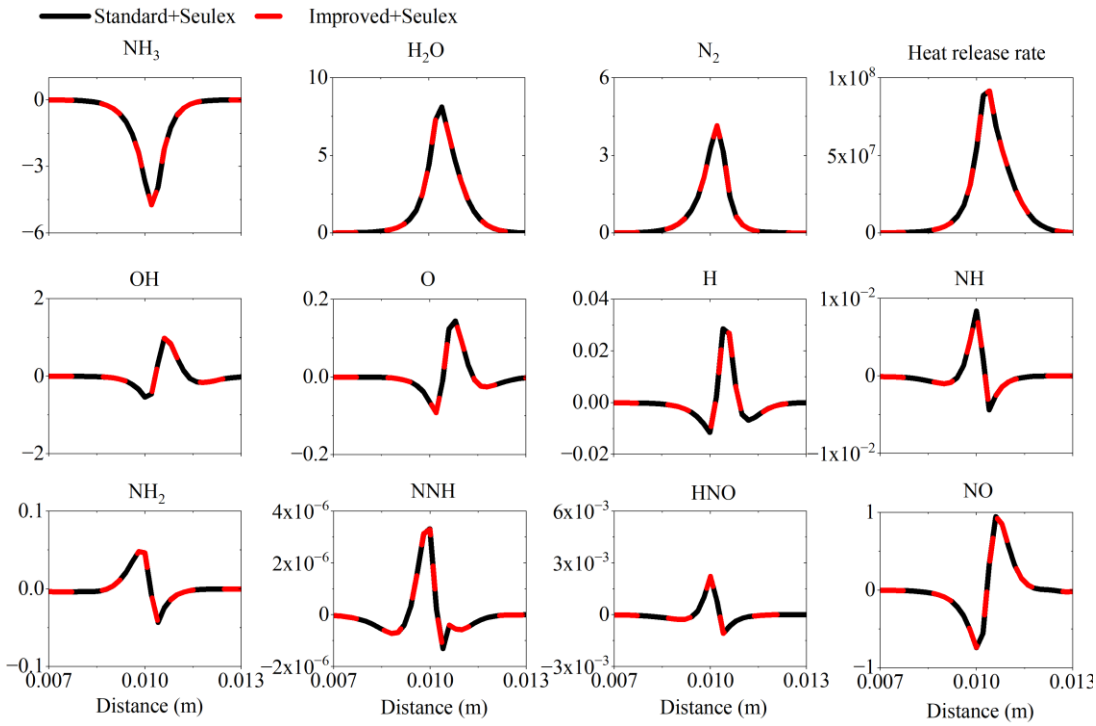

Fig. S18. Species production rate (kg/m^3/s) and heat release rate (W/m^3) profiles for counter flow flame of ammonia/air. The ODE algorithm is Seulex.

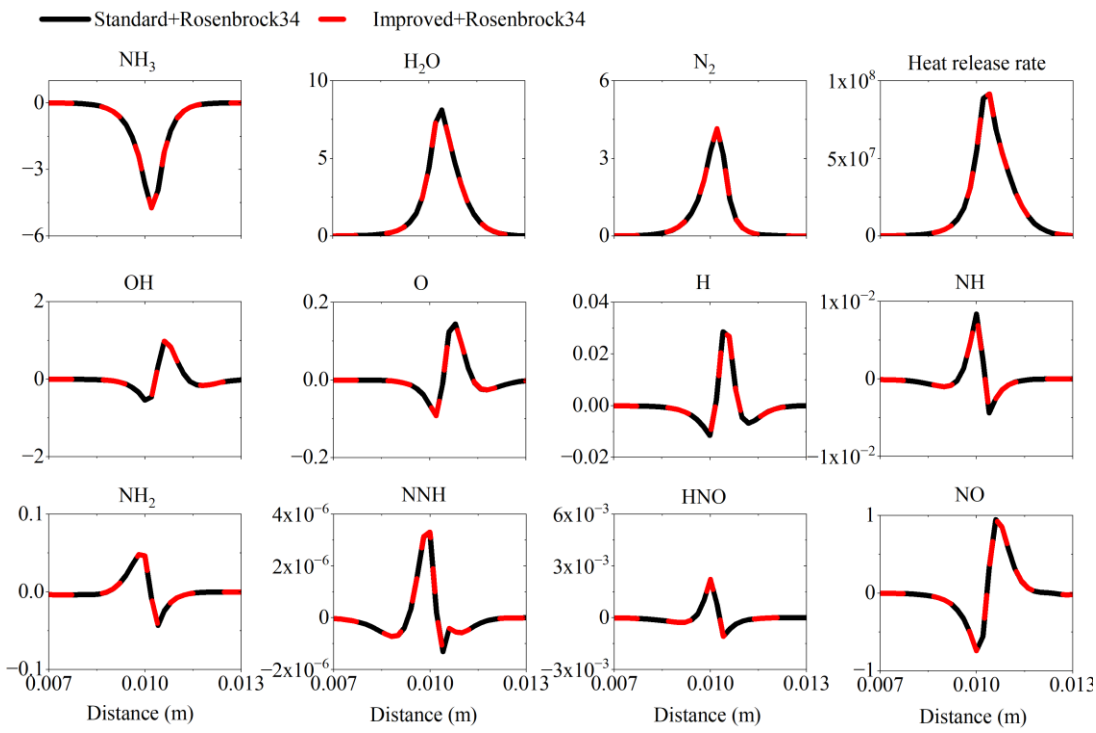

Fig. S19. Species mass fraction and temperature (K) profiles for counter flow flame of ammonia/air. The ODE algorithm is Rosenbrock34.

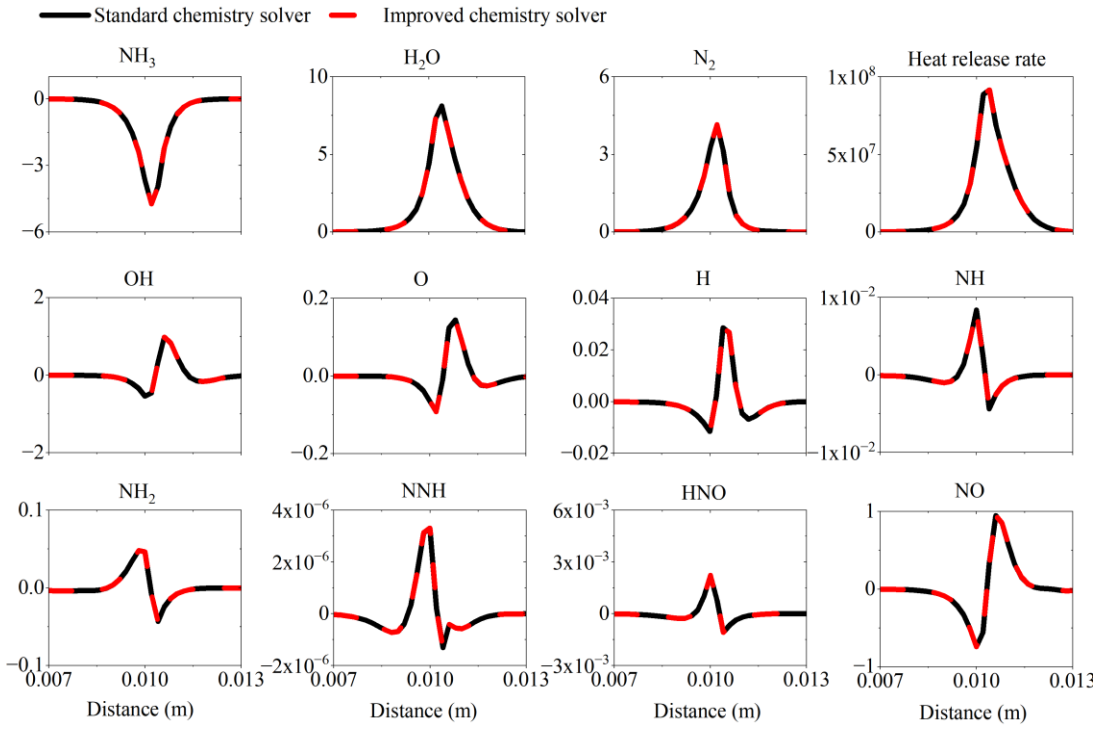

Fig. S20. Species production rate (kg/m^3/s) and heat release rate (W/m^3) profiles for counter flow flame of ammonia/air. The ODE algorithm is Rosenbrock34.

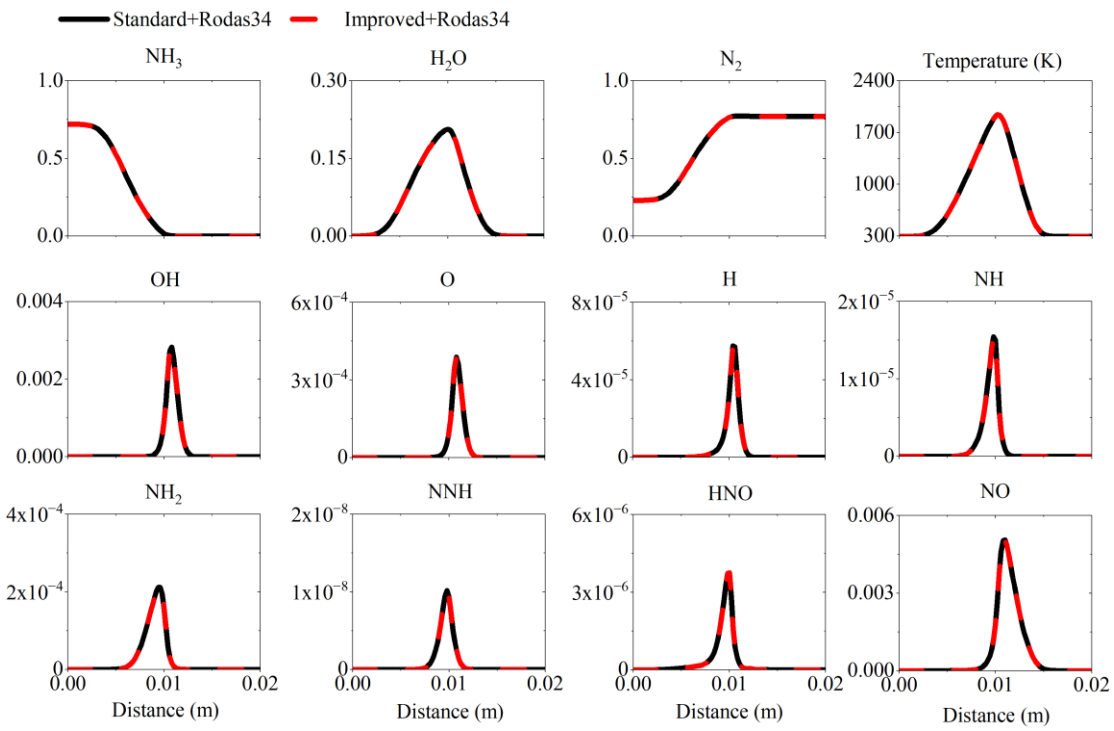

Fig. S21. Species mass fraction and temperature (K) profiles for counter flow flame of ammonia/air. The ODE algorithm is Rodas34.

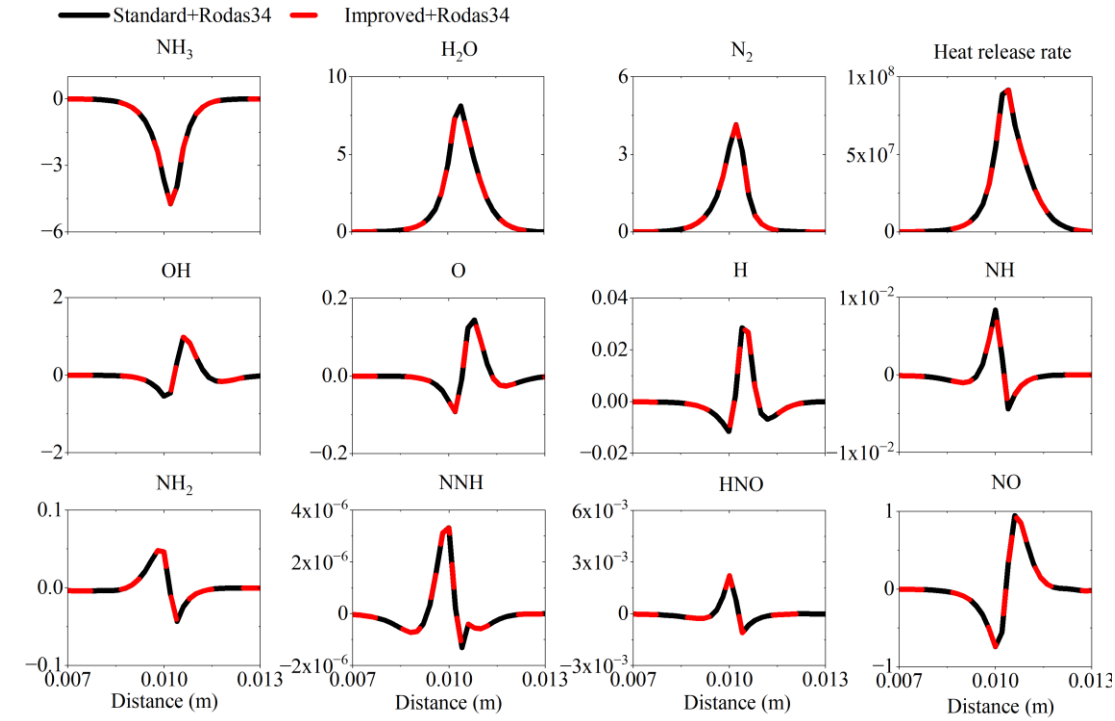

Fig. S22. Species production rate (kg/m^3/s) and heat release rate (W/m^3) profiles for counter flow flame of ammonia/air. The ODE algorithm is Rodas34.

2.3 N-dodecane

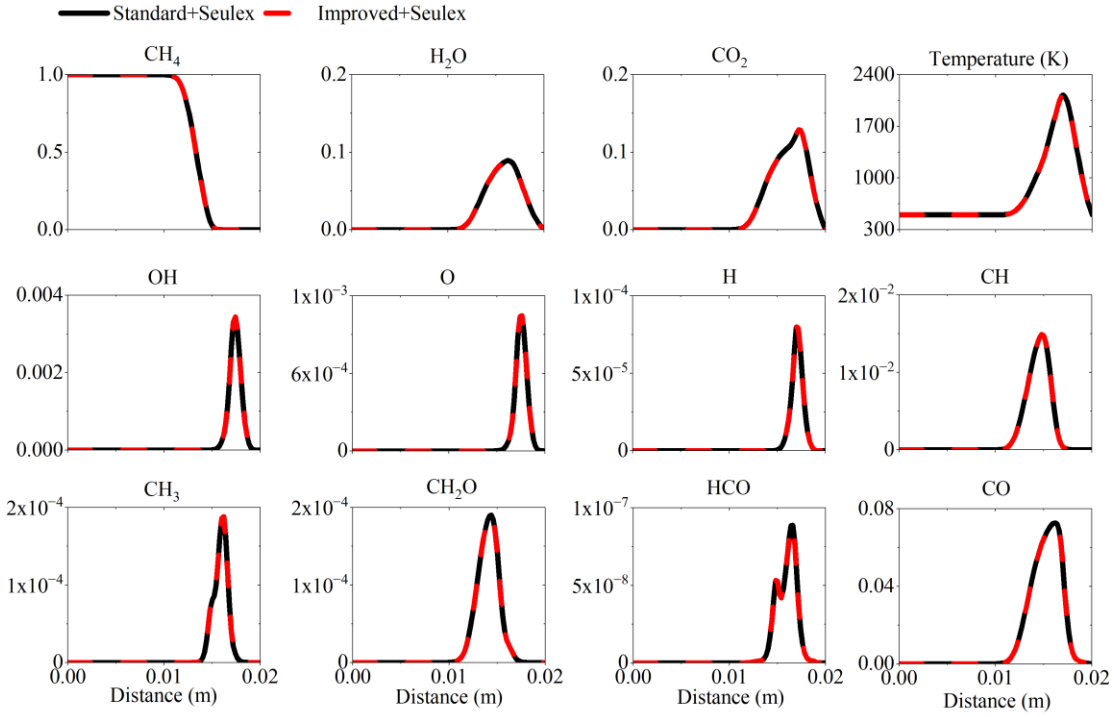

Fig. S23. Species mass fraction and temperature (K) profiles for counter flow flame of N-dodecane/air. The ODE algorithm is Seulex.

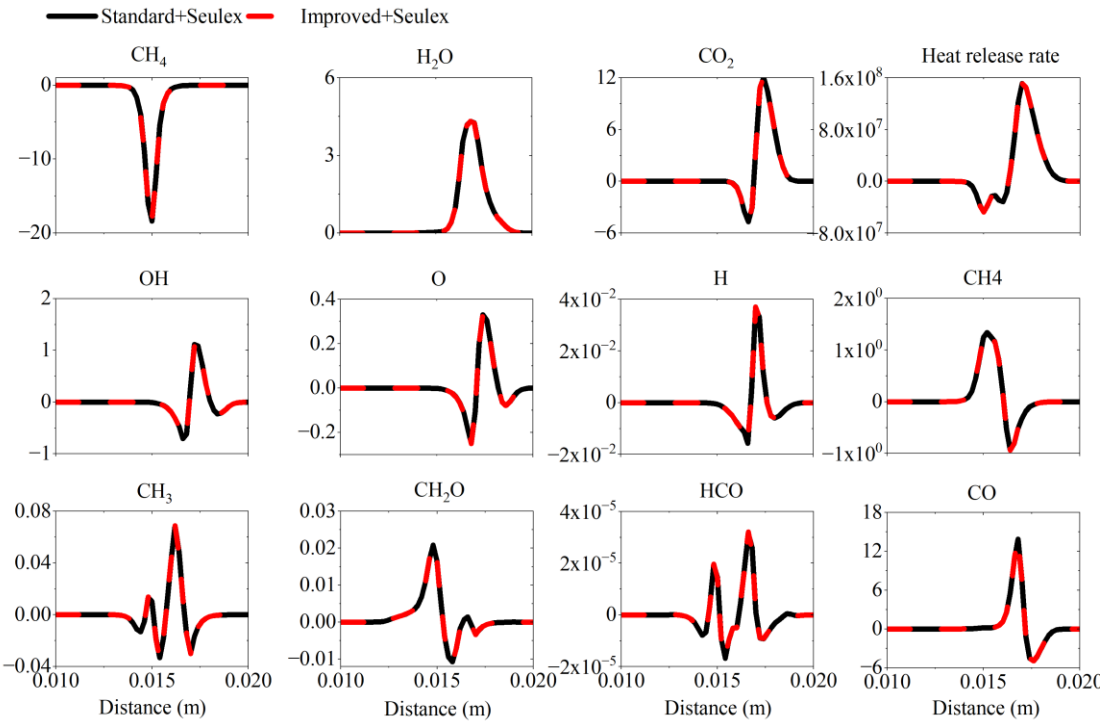

Fig. S24. Species production rate (kg/m^3/s) and heat release rate (W/m^3) profiles for counter flow flame of N-dodecane/air. The ODE algorithm is Seulex.

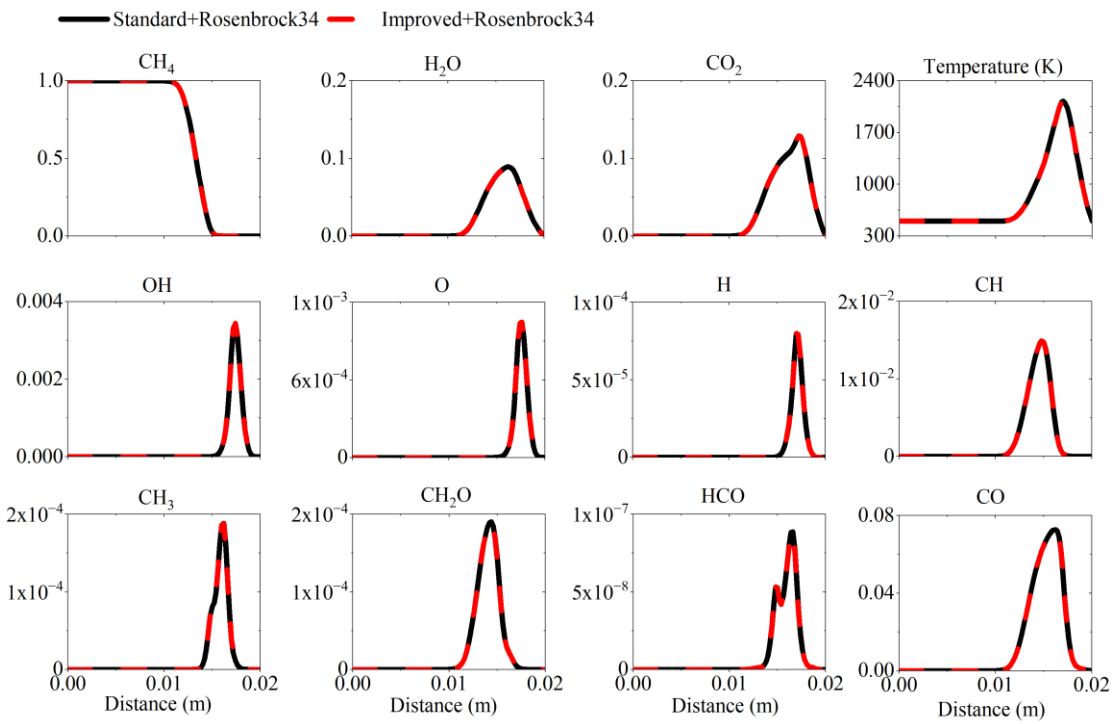

Fig. S25. Species mass fraction and temperature (K) profiles for counter flow flame of N-dodecane/air. The ODE algorithm is Rosenbrock34.

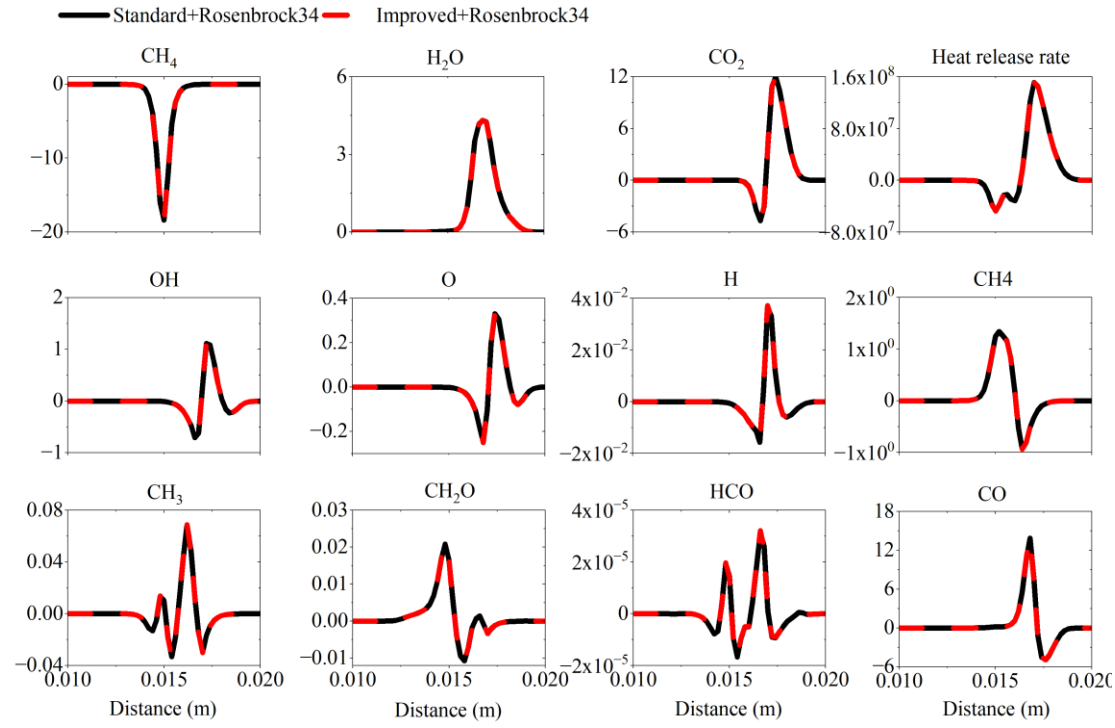

Fig. S26. Species production rate (kg/m^3/s) and heat release rate (W/m^3) profiles for counter flow flame of N-dodecane/air. The ODE algorithm is Rosenbrock34.

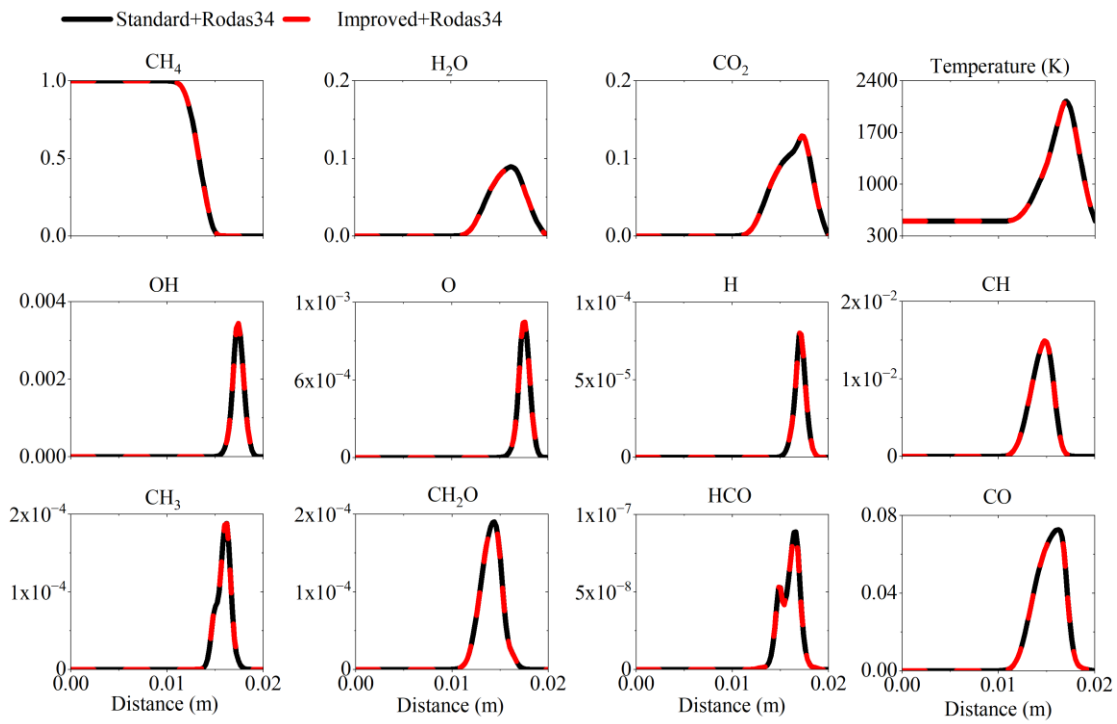

Fig. S27. Species mass fraction and temperature (K) profiles for counter flow flame of N-dodecane/air. The ODE algorithm is Rodas34.

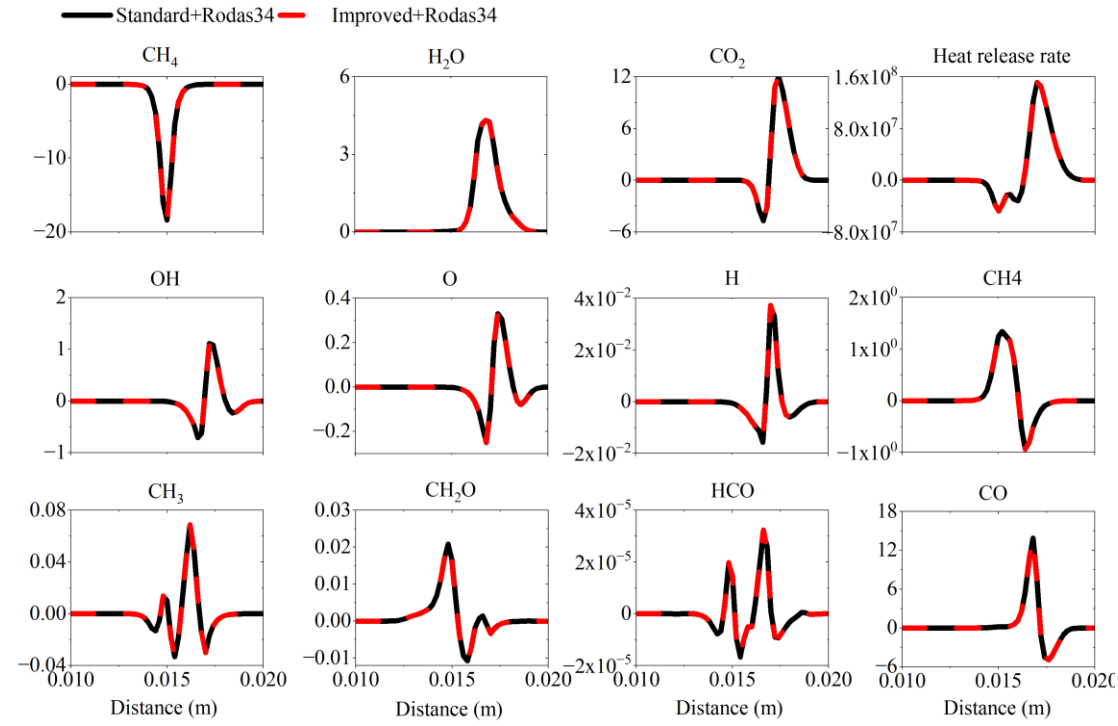

Fig. S28. Species production rate (kg/m^3/s) and heat release rate (W/m^3) profiles for counter flow flame of N-dodecane/air. The ODE algorithm is Rodas34.

Reference

[1] M. Ó Conaire, H. J. Curran, J. M. Simmie, W. J. Pitz, C. K. Westbrook. A comprehensive modeling study of hydrogen oxidation. Int. J. Chem. Kinet. 36 (2004) 603–622.

[2] A. A. Konnov. Yet another kinetic mechanism for hydrogen combustion. Combust. Flame 203 (2019) 14–22.

[3] A. Kazakov, M. Frenklach. Reduced Reaction Sets based on GRI-Mech 1.2.

[4] Gregory P. Smith, David M. Golden, Michael Frenklach, Nigel W. Moriarty, Boris Eiteneer, Mikhail Goldenberg, C. Thomas Bowman, Ronald K. Hanson, Soonho Song, William C. Gardiner, Jr., Vitali V. Lissianski, and Zhiwei Qin.

[5] G. Sahut, T. Nilsson, C. Fureby, et al. Large-Eddy Simulation of Supersonic Combustion in a Mach 2 Cavity-Based Model Scramjet Combustor. in AIAA SCITECH 2024 Forum (American Institute of Aeronautics and Astronautics, Orlando, FL, 2024).

[6] Chemical-Kinetic Mechanisms for Combustion Applications.

[7] S. Roy, O. Askari. A New Detailed Ethanol Kinetic Mechanism at Engine-Relevant Conditions. Energy Fuels 34 (2020) 3691–3708.

[8] N. M. Marinov. A detailed chemical kinetic model for high temperature ethanol oxidation. Int. J. Chem. Kinet. 31 (1999) 183–220.

[9] S. Liu, J. C. Hewson, J. H. Chen, H. Pitsch. Effects of strain rate on high-pressure nonpremixed n-heptane autoignition in counterflow. Combust. Flame 137 (2004) 320–339.

[10] T. Lu, C. K. Law, C. S. Yoo, J. H. Chen. Dynamic stiffness removal for direct numerical simulations. Combust. Flame 156 (2009) 1542–1551.

[11] T. Lu, C. K. Law. Diffusion coefficient reduction through species bundling. Combust. Flame 148 (2007) 117–126.

[12] A. Vié, B. Franzelli, Y. Gao, et al. Analysis of segregation and bifurcation in turbulent spray flames: A 3D counterflow configuration. Proc. Combust. Inst. 35 (2015) 1675–1683.

[13] T. Yao, Y. Pei, B.-J. Zhong, et al. A compact skeletal mechanism for n-dodecane with optimized semi-global low-temperature chemistry for diesel engine simulations. Fuel 191 (2017) 339–349.

[14] K. Narayanaswamy, P. Pepiot, H. Pitsch. A chemical mechanism for low to high temperature oxidation of n-dodecane as a component of transportation fuel surrogates. Combust. Flame 161 (2014) 866–884.

[15] C. S. Yoo, Z. Luo, T. Lu, H. Kim, J. H. Chen. A DNS study of ignition characteristics of a lean iso-octane/air mixture under HCCI and SACI conditions. Proc. Combust. Inst. 34 (2013) 2985–2993.

[16] H. Curran. A comprehensive modeling study of iso-octane oxidation. Combust. Flame 129 (2002) 253–280.

[17] N. Zettervall, C. Fureby, E. J. K. Nilsson. A reduced chemical kinetic reaction mechanism for kerosene-air combustion. Fuel 269 (2020) 117446.

[18] W. Yao, Y. Lu, K. Wu, J. Wang, X. Fan. Modeling Analysis of an Actively Cooled Scramjet Combustor Under Different Kerosene/Air Ratios. J. Propuls. Power 34 (2018) 975–991.

[19] R. S. Khare, S. K. Parimalanathan, V. Raghavan, K. Narayanaswamy. A comprehensively validated compact mechanism for dimethyl ether oxidation: an experimental and computational study. Combust. Flame 196 (2018) 116–128.

[20] A. Bhagatwala, Z. Luo, H. Shen, et al. Numerical and experimental investigation of turbulent DME jet flames. Proc. Combust. Inst. 35 (2015) 1157–1166.
[21] S. L. Fischer, F. L. Dryer, H. J. Curran. The reaction kinetics of dimethyl ether. I: High-temperature pyrolysis and oxidation in flow reactors. Int. J. Chem. Kinet. 32 (2000) 713–740.
[22] E. C. Okafor, Y. Naito, S. Colson, et al. Experimental and numerical study of the laminar burning velocity of CH4–NH3–air premixed flames. Combust. Flame 187 (2018) 185–198.
[23] X. Zhang, S. P. Moosakutty, R. P. Rajan, M. Younes, S. M. Sarathy. Combustion chemistry of ammonia/hydrogen mixtures: Jet-stirred reactor measurements and comprehensive kinetic modeling. Combust. Flame 234 (2021) 111653.